Screening by Kinetic Monte Carlo Simulation of Pt−Au(100) Surfaces for the Steady-State Decomposition of Nitric Oxide in Excess Dioxygen[†]

Laurent D. Kieken,*,‡ Matthew Neurock,*,§ and Donghai Mei§

NovoDynamics, Inc., 123 North Ashley Street, Suite 210, Ann Arbor, Michigan 48104, and Department of Chemical Engineering, University of Virginia, Charlottesville, Virginia 22904-4741

Received: March 14, 2004; In Final Form: October 8, 2004

An ab initio-based kinetic Monte Carlo algorithm was developed to simulate the direct decomposition of NO over Pt and different PtAu alloy surfaces. The algorithm was used to test the influence of the composition and the specific atomic surface structure of the alloy on the simulated activity and selectivity to form N_2. The apparent activation barrier found for the simulation of lean NO decomposition over Pt(100) was 7.4 kcal/mol, which is lower than the experimental value of 11 kcal/mol that was determined over supported Pt nanoparticles. Differences are likely due to differences in the surface structure between the ideal (100) surface and supported Pt particles. The apparent reaction orders for lean NO decomposition over the Pt(100) substrate were calculated to be 0.9 and −0.5 for NO and O_2, respectively. Oxygen acts to poison Pt. Simulations on the different Pt−Au(100) surface alloys indicate that the turnover frequency goes through a maximum as the Au composition in the surface is increased, and the maximum occurs near 44% Au. Turnover frequencies, however, are dictated by the actual arrangements of Pt and Au atoms in the surface rather than by their overall composition. Surfaces with similar compositions but different alloy arrangements can lead to very different activities. Surfaces composed of 50% Pt and 50% Au (Pt_4 and Au_4 surface ensembles) showed very little enhancement in the activity over that which was found over pure Pt. The Pt−Pt bridge sites required for NO adsorption and decomposition were still effectively poisoned by atomic oxygen. The well-dispersed $Pt_{50\%}Au_{50\%}$ alloy, on the other hand, increased the TOF over that found for pure Pt by a factor of 2. The most active surface alloy was one in which the Pt was arranged into "+" ensembles surrounded by Au atoms. The overall composition of this surface is $Pt_{56.2\%}Au_{43.8\%}$. The unique "+" ensembles maintain Pt bridge sites for NO to adsorb on but limit O_2 as well as NO activation by eliminating next-nearest neighbor Pt-bridge sites. The repulsive interactions between two adatoms prevent them from sharing the same metal atoms. The decrease in the oxygen coverage leads to a greater number of vacant sites available for NO adsorption. This increases the NO coupling reaction and hence N_2 formation. The inhibition of the rate of N_2 formation by O_2 is therefore suppressed. The coverage of atomic oxygen decreases from 53% on the Pt(100) surface down to 19% on the "+" ensemble surface. This increases the rate of N_2 formation by a factor of 4.3 over that on pure Pt. The reaction kinetics over the "+" ensemble $Pt_{56.2\%}Au_{43.8\%}$ surface indicate apparent reaction orders in NO and oxygen of 0.7 and 0.0, respectively. This suggests that oxygen does not poison the PtAu "+" alloy ensemble. The activity and selectivity of the PtAu ensembles significantly decrease for alloys that go beyond 60% Au. Higher coverages of Au shut down sites for NO adsorption and, in addition, weaken the NO and O bond strengths, which subsequently promotes desorption as well as NO oxidation. The computational approach identified herein can be used to more rapidly test different metal compositions and their explicit atomic arrangements for improved catalytic performance. This can be done "*in silico*" and thus provides a method that may aid high-throughput experimental efforts in the design of new materials. The synthesis and stability of the metal complexes suggested herein still ultimately need to be tested.

Introduction

The development of new high-throughput experimentation (HTE) tools for heterogeneous catalyst synthesis, characterization, and screening enables catalytic scientists to increase productivity and expand the experimental phase space that they can explore. At the same time, these tools place a greater burden on the scientist to plan experiments that extract useful knowledge from the large amount of data that can be utilized to guide and advance catalyst development. Various approaches to guiding catalyst development have been applied to HTE and are reviewed by Caruthers et al.[1] They fall into two general methodologies, which are often complementary in HTE catalyst development efforts. In the first methodology, the catalyst is typically treated as a "black box", and machine learning techniques are used to model catalyst activity or selectivity as a function of experimental variables in order to find combinations of these variables that optimize performance. This approach generates little fundamental understanding but may be useful in correlating the effects of composition or process variables.

For example, Baerns et al.[2,3] have used genetic algorithm to optimize the composition of catalyst materials to increase activity of the oxidative dehydrogenation of propane. Similarly, Serra et al.[4] have applied artificial neural networks to model kinetic data for the hydroisomerization of various n-paraffins as a function of reactor process conditions. The second methodology is based on the microkinetic analysis of the catalytic cycle to describe the activity and selectivity of the catalyst in terms of the rate constants of the presumed elementary steps of the reaction.[5] These rate constants are typically measured, extrapolated from surface science experiments, or calculated using computational chemistry. While microkinetic analysis requires a significant input of kinetic and spectroscopic information, it allows one to calculate the activity and selectivity of the catalyst and to identify the elementary steps in the catalytic cycle that the activity (or selectivity) is most sensitive to. As described by Boudart,[6] the microkinetic analysis becomes the "knowledge base of combinatorial catalysis through the screening process". The set of rate constants can be improved at each iteration of the catalyst screening cycle, until lead candidate catalysts are identified for more in-depth testing. The application of microkinetic analysis to guide catalyst development, however, is still a considerable challenge. Deterministic models which drive most microkinetic efforts are typically based on rate constants that are averaged over the surface structure and thus devoid of the structural information necessary for design.

First-principles-based kinetic Monte Carlo (KMC) simulation is a tool that can assist in bridging this gap in catalyst development efforts since it can relate catalyst activity and selectivity to systematic changes in the atomic and electronic structure of the catalytic surface. Kinetic Monte Carlo simulation explicitly tracks the temporal behavior of all the surface species as a function of time, surface site configurations, and reaction conditions. Neurock et al.[7−14] have shown how density functional theoretical (DFT) methods can be coupled with kinetic Monte Carlo simulation in order to construct a first-principles-based kinetic simulation that can follow the temporal behavior at the catalyst surface and thus model activity and selectivity. This combined DFT−KMC approach maintains the atomic structure of the catalytic surface and can therefore be used to probe how changes in that surface impact catalytic performance. The approach has been used successfully to simulate various catalytic systems.[7−14]

Herein we show how this approach can also be used in a semiquantitative predictive manner in order to examine how changes in the metals, alloy compositions, and even the specific arrangements of the atoms within the surface ensemble influence catalytic activity. Randomly dispersed surface alloys were constructed herein and screened for their catalytic performance. We specifically target the decomposition of NO under lean operating conditions. Our goal is not to simulate the behavior of bulk particles of Pt and Au which have a limited range of compositions but instead try to identify specific atomic assemblies that might be active, regardless of whether they can currently be produced or stabilized. The results from these studies suggest specific atomic assemblies that one might try to synthesize and stabilize under reaction conditions.

Background: NO Decomposition

The low rates reported for the catalytic NO decomposition under excess dioxygen are the primary limitation to the potential application of this reaction for the removal of NO from the exhaust s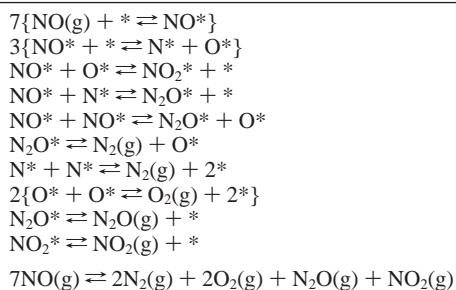tream of lean-burn engines. Lean-burn engines are advantageous because they provide a significantly better fuel economy than traditional combustion engines, but they require a different solution for NO_x removal than use of the current three-way catalysts, which fail to reduce NO_x concentrations in engine effluent streams to regulated levels. Cu-exchanged ZSM-5 catalysts are among the most active NO decomposition catalysts reported.[15] However, zeolites suffer from hydrothermal stability[16] issues and from SO_2 poisoning.[17] Supported platinum catalysts are less active than Cu−ZSM-5 catalysts but they typically resist SO_2 poisoning better and are more stable at high temperatures. The kinetics of NO decomposition has been studied for Pt/Al_2O_3 between 873 and 973 K, and on Pt foils between 973 and 1323 K, at 760 to 1530 Torr by Amirnazmi and co-workers.[18,19] The reactant gas contained from 1.5 to 15% NO and from 0 to 5% O_2. In the presence of inlet O_2 gas, the rate was found to be proportional to NO concentration and the reaction order in O_2 was negative one. The oxygen inhibition was explained by the equilibrated chemisorption of oxygen on sites required for NO decomposition. Mummey and Schmidt,[20] who measured steady-state rates of NO decomposition in NO−O_2 gas mixture on polycrystalline Pt between 550 and 1700 K at 0.001 to 30 Torr, also reported this strong inhibition by oxygen.

Alloying the primary metal with an inert group IB metal is a classic solution to minimizing surface poisoning and thus increasing activity. Lam et al.,[21] for example, showed that alloying Au into Pd resulted in a significant increase in the turnover rate of the H_2−O_2 reaction in excess O_2, with a maximum at ∼60 atomic % Au. This rate increase is due to the decrease in the binding energy of oxygen on Pd with increasing amounts of Au. Wu et al.[22] reported an increase by 30−40% in the specific rate of NO decomposition on Pd−Au (5% Au) and Pd−Ag (10% Ag) supported on alumina catalysts relative to pure Pd, at 1173 K, atmospheric pressure, and NO inlet concentration of 4%. Pt metal is still one of the preferred metals for NO_x decomposition under lean conditions since it can activate NO and offers some resistance to poisoning. Bimetallic Pt−Au systems are therefore a natural place to start our efforts. Amiridis et al. used supported PtAu particles to study the selective catalytic reduction of NO in the presence of a sacrificial hydrocarbon reductant.[23] They show that SCR is inhibited by the addition of Au. Au in this system shuts down sites necessary to carry out the hydrocarbon activation. Skelton et al.[24] recently examined the influence of Au on NO and O_2 decomposition over Pt(335) substrates for sensor applications. Their results nicely show that gold poisons the step edge sites on the Pt-(335) surface. This shuts down NO dissociation sites, which acts to reduce N_2 formation. Oxygen, however, continues to dissociate over the (111) terrace sites. As far as we are aware, there have been no studies reported on the catalytic NO_x decompostion under lean conditions over supported bimetallic PtAu alloys.

In the present study we use a DFT-based kinetic Monte Carlo scheme to simulate the steady-state turnover frequency (TOF) of NO decomposition on Pt−Au(100) surfaces of various Au contents and spatial arrangements of the Pt and Au atoms to investigate whether alloying Au with Pt can reduce the oxygen inhibition of the rate of NO decomposition by preventing oxygen from poisoning the surface. The results are explained by changes in binding energy of oxygen and NO at steady-state conditions and by the atomic structure of the Pt−Au(100) surface.

Theoretical Calculations and Simulations

1. Reaction Mechanism. NO decomposition can proceed either from the direct dissociation to form nitrogen and oxygen

TABLE 1: Speculated reaction mechanism for the direct catalytic decomposition of NO over Pt(100)[a]

$$7\{NO(g) + * \rightleftharpoons NO*\}$$
$$3\{NO* + * \rightleftharpoons N* + O*\}$$
$$NO* + O* \rightleftharpoons NO_2* + *$$
$$NO* + N* \rightleftharpoons N_2O* + *$$
$$NO* + NO* \rightleftharpoons N_2O* + O*$$
$$N_2O* \rightleftharpoons N_2(g) + O*$$
$$N* + N* \rightleftharpoons N_2(g) + 2*$$
$$2\{O* + O* \rightleftharpoons O_2(g) + 2*\}$$
$$N_2O* \rightleftharpoons N_2O(g) + *$$
$$NO_2* \rightleftharpoons NO_2(g) + *$$

$$7NO(g) \rightleftharpoons 2N_2(g) + 2O_2(g) + N_2O(g) + NO_2(g)$$

[a] The elementary steps and their stoichiometric coefficients are given for each reaction step.

TABLE 2: for the atomization energies and binding energies for proposed species on Pt(100)

species	atomization energy (kcal/mol)	binding energy (kcal/mol)		
		atop	bridge	4-fold hollow
oxygen (O₂)				
nitrogen (N₂)				
nitrogen (N)			−96.3	−99.0
oxygen (O)			−94.2	−85.9
nitric oxide (NO)	160.5	−32.6	−51.2	−37.7
nitric dioxide (NO₂)	256.5	−28.4	−17.8	
nitrous oxide (N₂O)	292.9	−6.3	−2.8	

from simple statistical mechanics estimates, as will be described later in this paper.

2. Intrinsic Kinetics and Lateral Interactions. A kinetic database for all of the elementary steps proposed in Table 1 was constructed from the results of ab initio quantum mechanical calculations. Plane wave gradient corrected periodic DFT calculations were performed using the VASP code developed by Kresse and Hafner[38,39] in order to determine the adsorption energies of all reactant, intermediates, and products on the Pt-(100) surface at different coverages. The overall reaction energies along with the activation barriers for each of the elementary steps outlined in Table 1 were subsequently calculated at different surface coverages. More specifically, all of the results described herein were calculated using the Perdew–Wang form of the generalized gradient approximation (GGA) to determine exchange and correlation corrections.[40] The metal surface was described by using a periodic supercell which contained between 4 and 6 metal layers along with a 12 Å vacuum layer to electronically separate the repeating slab structure in the z-direction. The top layers of the slab, as well as the adsorbate structure, were allowed to freely optimize. The bottom layer of the slab was held fixed at the bulk lattice spacing of the metal. Transition states were isolated using a nudged elastic band technique.[41]

The results from the calculations of NO on Pt(100) are summarized in Tables 2–3 below. The atomization energies as well as the adsorption energies for all of the intermediates proposed in the mechanism are presented in Table 2. The binding energies for each adsorbate were calculated at different sites on the surface to identify the most stable adsorption sites. The forward as well as the reverse activation barriers for all of the steps proposed in Table 1 were calculated on Pt(100). The results are presented in Table 3. A more detailed discussion of the results summarized here can be found in refs 14, 27, 33, and 34. The preexponential factors for all of the surface reaction and desorption steps along with the sticking coefficients for all adsorption steps are also given in Table 3. This is discussed in more detail in the section on rate calculations that follows. Ab initio DFT thus provides for a detailed intrinsic kinetic database that describes NO decomposition over Pt(100). This is necessary for establishing a quantitative basis for the pure Pt system. The database is therefore subsequently used to simulate the kinetics for NO decomposition under lean conditions over Pt(100) as described in the Results section.

Influence of Au. The influence of Au is treated as a perturbation to the results for pure Pt. In principle, one could carry out similar sets of detailed quantum mechanical calculations on a full range of different PtAu alloys to establish the kinetics on each of these surfaces. Unfortunately the number of different PtAu configurations that could hypothetically be formed would make it computationally intractable to examine from ab initio calculations alone. We have therefore developed a DFT-modified bond order conservation approach that can be

adatoms or from the coupling of two NO molecules to form N₂O, which can subsequently react at higher temperatures to form N₂ and chemisorbed atomic oxygen. The results from ultrahigh vacuum studies as well as theoretical studies of NO on different Pt substrates indicate that NO activation likely proceeds over more open surfaces and at more coordinatively unsaturated sites.[14,25–28] It is well established that NO will adsorb and react on Pt(100) to form N₂ and O₂ at lower coverages.[29–31] TPD experiments on Pt(100) show the desorption of NO, N₂, and O₂ where 25% of the surface adlayer decomposes. At higher coverages, NO dissociation becomes limiting. NO coupling therefore begins to compete with direct dissociation and may actually win out in terms of N₂ production.[25–27] A series of surface reaction steps that includes both NO dissociation, NO coupling, adsorption, and desorption steps has been assembled into a potential mechanism. The elementary steps that make up this mechanism are presented in Table 1.[14] The site preferences and adsorption energies for all of the species speculated in the mechanism proposed in Table 1 were calculated using ab initio density functional theory. The results along with the specific features of the calculations are presented elsewhere in detail.[14,27] The important findings for the simulations undertaken herein are summarized below in the section on "Intrinsic Kinetics".

The mechanism proceeds via the molecular adsorption of NO and O₂. NO can bind to any one of the available surface sites (atop, 2-fold bridge, 4-fold hollow). Both theory and experiment indicate that at lower surface coverages, NO prefers to bind to the Pt-bridge site.[25–27,33–34] It is assumed that O₂ adsorbs in a precursor state. At the higher temperatures of operation, the lifetime in this precursor state is very short-lived. Molecular oxygen either reacts to form two oxygen adatoms (O*) or simply desorbs as O₂. We, therefore, do not explicitly track the precursor state of oxygen in the simulations reported herein as it would have little effect on the resulting kinetics. The atomic oxygen that forms upon O₂ dissociation prefers to adsorb at bridge sites on the Pt(100).[14,33–34,37] Adsorbed NO subsequently dissociates to form atomic nitrogen and oxygen. Atomic nitrogen can sit at either the bridge or the hollow sites but has a stronger preference for the 4-fold hollow sites. In addition, adsorbed NO can react with neighboring oxygen atoms or nitrogen atoms to form NO₂ or N₂O, respectively. DFT results indicate that the atop sites are the most favorable sites for adsorbed NO₂ and N₂O on the Pt(100) surface.[14] The adsorbed NO₂ and N₂O can either undergo subsequent surface reactions or desorb from the surface. Two atomic oxygen or nitrogen atoms can recombine and desorb as O₂ and N₂, respectively. Density functional theory was used to calculate the activation barriers for the forward and the reverse paths for all of the steps presented in Table 1. The DFT barriers serve as input to the KMC simulations over Pt. The Arrhenius preexponential factors for each step were derived

TABLE 3: Activation barriers (E_{for} and E_{rev}) and the prexponential factors (ν_{for} and ν_{rev}) or sticking coefficients (s_o) for the forward and reverse elementary steps[a]

reaction	E_{for} (kcal/mol)	E_{rev} (kcal/mol)	ν_{for} (s^{-1})	$s_{o\ for}$ s^{-1}	ν_{rev} (s^{-1})	$s_{o\ rev}$ (s^{-1})
NO (g) + * ↔ NO*	0.0	51.2	-	0.7	1×10^{13}	-
NO* + * ↔ N* + O*	25.6	5.0	1×10^{13}	-	1×10^{13}	-
NO* + O* ↔ NO$_2$ * + *	31.7	11.7	1×10^{13}	-	1×10^{13}	-
NO* + N* ↔ N$_2$O* + *	33.9	22.2	1×10^{13}	-	1×10^{13}	-
NO* + NO* ↔ N$_2$O* + O*	37.5	0.0	1×10^{13}	-	1×10^{13}	-
N$_2$O* ↔ N$_2$(g) + O*	0.0	24.6	1×10^{13}	-	1×10^{13}	-
N* + N* ↔ N$_2$(g) + 2*	9.0	33.7	1×10^{13}	-	-	0.1
O* + O* ↔ O$_2$ (g) + 2*	0.0	52.2	1×10^{13}	-	-	0.1
NO$_2$* ↔ NO$_2$ (g) + *	28.4	0.0	1×10^{13}	-	-	1.0
N$_2$O* ↔ N$_2$O(g) + *	6.3	0.0	1×10^{13}	-	-	1.0

[a] All reaction steps and desorption steps are described by preexponential factors, whereas all adsorption reactions are defined using sticking probabilities. The activation barriers reported here were calculated from first-principle DFT calculations over Pt(100) reported earlier[14,26] in the literature. The preexponential factors were estimated from statistical mechanics and the sticking coefficients were taken based on typical values for dissociative and molecular sticking coefficients from the literature[35] and previous microkinetic modeling studies for NO on Pt.[32]

used to provide estimates for the alloys. The method is constructed using the ab initio results calculated for Pt and subsequently extended to treat PtAu.

An integral part of describing the surface reaction kinetics involves accounting for the effects of the local environment on the kinetics at the active sites. The lateral interactions that take place between two or more adsorbates can be characterized as either *through-space* interactions, which are those interactions that are due to coulombic and/or steric effects, or *through-surface* interactions, which are those that result from charge transfer between the adsorbate and metal atoms. These interactions play an important role in dictating the heats of adsorption and surface kinetics as shown from NO TPD and calorimetric experiments on different metal surfaces.[35,42] In this work, we model the through-space interactions by using van der Waals (vdW) interaction terms from the Merck molecular force field.[43] The through-surface interactions are calculated using a DFT-scaled BOC method[7−9] for the adsorbed N, O, NO, N$_2$O, and NO$_2$ intermediates on Pt(100). This model was derived by parameterizing a bond order conservation model to fit density functional theory results on Pt. DFT was used to establish the influence of surface coverage on the adsorption as well as the reaction energies. In general, increasing the surface coverage decreased the calculated adsorption energy.

It would be impossible to calculate the 1×10^6 or more conceivable interaction configurations and alloys that could arise at the surface from density functional theory. The DFT-based BOC model thus provides for reliable descriptions of the binding energies and activation barriers to be calculated much more rapidly. The model developed on Pt is extended here to more rapidly screen a number of different potential Pt−Au alloys. The results on PtAu are primarily based on BOC estimates and are therefore only semiquantitative. A modified bond order conservation method is used to calculate the adsorption energies and the activation energies for all proposed elementary steps occurring on bimetallic sites. The Au−O (45.0 kcal/mol) and Au−N (58.2 kcal/mol) bond strengths were taken directly from Shustorovich and Sellers.[44] DFT-calculated binding energies for N and O on Au(100) were found to be consistent with the initial BOC values from Shustorovich and Sellers. The values for the Au−N and Au−O binding energies thus provide the basis for BOC to determine the binding energies for all of the other intermediates at different sites on the Au(100) surface. The results for the binding energies on Pt and Au were subsequently used in a modified BOC approach to calculate the binding energies and activation barriers on the alloy surfaces.[45]

3. Rate Calculation

The reaction rate constant k_i for each elementary step is calculated using transition state theory

$$k_i = \nu_i \exp\left(\frac{-\Delta E_i}{RT}\right) \tag{1}$$

where R is the gas constant, T is the temperature, and ΔE_i and ν_i refer to the activation energy barrier and the Arrhenius prefactor for the elementary step i. The activation barriers for all of the elementary steps have been determined by DFT calculations over the Pt(100) surface. The barriers over the Pt−Au(100) surface were estimated using the modified BOC approach presented above. The details of this approach can be found in previous publications.[7,8,12]

The preexponential factors, ν_i, were derived from statistical mechanical estimates. Unimolecular surface decomposition reactions are typically 10^{13} s^{-1}.[45] All unimoleucar decomposition steps were thus chosen to have a values of 10^{13} s^{-1}. The preexponential factor for bimolecular surface reactions of the form A* + B*, where A and B are immobile, is calculated for a deterministic system to be 10^{-2} or 10^{-3} cm^2/s.[46−47] The deterministic rate equation for a bimolecular system, however, must also be multiplied by the site density (10^{15} sites/cm^2) in order to provide the preexponential factor in terms of s^{-1}. This is necessary for atomic scale simulations. The apparent preexponential factor for the reaction of A* + B* then becomes 10^{13} s^{-1}. This is consistent with both theoretical and experimental values reported in the literature.[26,46,48] Desorption was also modeled using a value of 10^{13} s^{-1}. This can also be found in most classic statistical mechanical estimations for desorption.[46,48] The further distinction between unimolecular and bimolecular steps based on differences in the vibrational modes between the transition and the reactant states is not made herein. This can in principle best be determined by detailed ab initio calculations using the explicit forces that act upon each state. These differences were not thought to be major contributions or essential for screening purposes and therefore were not followed.

The preexponential factor for the molecular desorption of O$_2$ was assumed to be 10^{15} s^{-1}.[49] The calculation of adsorption rate is characteristically different from the surface elementary reaction rate calculations. The adsorption rate for species i is defined as

$$r_{ad,i} = s_0 \cdot P_i \cdot A_S \cdot (2\pi \cdot MW_i \cdot RT)^{-0.5} \exp\left(\frac{-\Delta E_i}{RT}\right) \tag{2}$$

where s_0 is the sticking coefficient, P_i is the partial pressure of species i, A_s is the area of one surface site, and MW_i is the molecular weight of species i.[10,11] The sticking coefficients of NO, N_2O, and NO_2 were taken to be 0.7, 1.0, and 1.0, respectively. The sticking coefficient of O_2 was assumed to be 0.1. These values were chosen based on previous surface science[35] and microkinetic modeling results[32] for NO decomposition and oxidation on Pt.

The sticking coefficients were modeled using classical collision theory and thus allowed to change with temperature via a kinetic theory of gases, as is shown above in eq 2. The sticking coefficient increases with temperature according to $T^{0.5}$. The surface reactions, however, were modeled using transition state theory. As a first-order approximation, we assumed that the changes in the partition function with respect to temperature were constant and that all changes in the rate constant arise from $\exp(-\Delta H^{\ddagger}/RT)$. The preexponential factors were therefore held constant with temperature. This is an assumption in the simulation since preexponential factors can change with large changes in temperature.[26]

4. Kinetic Monte Carlo Simulation

Kinetic Monte Carlo simulation tracks the individual molecular transformations as a function of time and processing conditions. The details of the algorithm were described previously.[7−14] Only a brief description of the approach is outlined here. In this paper, we focus solely on simulating the (100) surface, which is represented by a 12 × 12 atom grid containing over 144 sites. We found very small changes in the reported kinetics in increasing the grid size to a 32 × 32 system (1024 sites). The 12 × 12 grid was therefore thought to be appropriate for carrying out screening simulations over different alloy surfaces. Periodic boundary conditions were used in all of the simulations. Structural, electronic, and energetic properties calculated from DFT for all of the intermediates on Pt(100) were used as input into the simulation. This intrinsic kinetic database was subsequently combined with the lateral interaction model and incorporated into the core reaction model in the simulation. The surface is initially constructed to identify all possible sites and surface events. After this initialization, all surface sites are stochastically sampled in order to construct a cumulative reaction probability distribution that outlines all the possible kinetic events that can occur. This includes adsorption, surface reaction, surface diffusion, and desorption. The events that are considered depend on the specific surface site of occurrence and its surrounding reaction environment. For each surface reaction event, the simulation determines the binding energies of reactants as well as the possible product states from either a direct DFT lookup table or via the BOC model. These adsorption energies are then used to calculate the overall energetics and the effects of reaction environment. The activation barriers for each step are calculated by combining the intrinsic results determined from DFT with the through-surface and through-space interaction energies calculated from BOC and the MMFF model, respectively. At any instant in time, t_i, the rates for all possible events are added up in order to determine the total rate. The total rate, Σr_i, is used in the variable time-step equation (eq 3) to determine the time at which the next possible event on the surface occurs

$$\Delta t_v = \frac{-\ln(RN)}{\sum_i r_i} \tag{3}$$
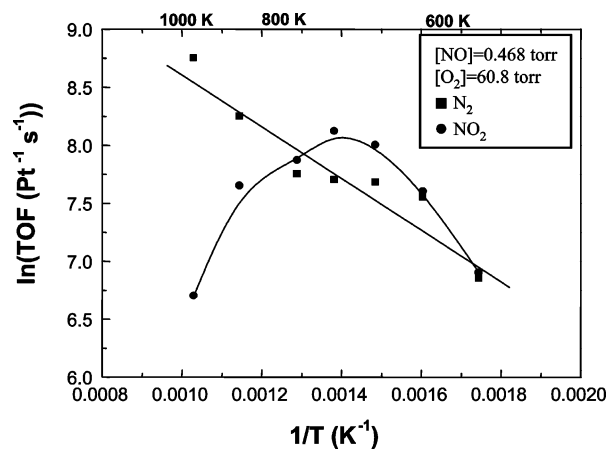
Figure 1. Simulated turnover frequencies for the formation of N_2 and NO_2 over Pt(100). The partial pressures of NO and O_2 were 0.468 and 60.8 Torr, respectively. The symbols are as follows: (●) NO_2; (■) N_2.

where Δt_v is the variable time step and RN is a random number between 0 and 1. The specific reaction that occurs within the calculated time step interval is chosen based on the cumulative reaction probability distribution s_i

$$s_i = \frac{r_i}{\sum_i r_i} \tag{4}$$

The outcome from the simulation includes the detailed structure and composition of the surface adlayer along with the gas-phase composition as a function of time and processing conditions. This temporal and spatial resolution of the surface enables us to compute a range of different properties, including molecular or site-explicit turnover frequencies, activation barriers, surface coverages, and other overall averaged energetic properties, under reaction conditions. The turnover frequency (TOF) for molecule i was calculated by counting the number of i molecules that desorb from the surface as a function of time per surface Pt atom in the array. Apparent activation barriers and reaction orders for the overall reaction can be calculated by running the KMC simulation at different temperatures and partial pressures of reactants as it is done in an experiment.

The error in the estimate of the overall reaction and the activation energies from density functional theory is on the order of 4 to 7 kcal/mol. This error estimate is for a single elementary step, the error in simulating overall catalytic kinetics can be greater. We have seen, however, that there tends to be cancellation of errors in simulating overall catalytic cycles. Our goal in this work, however, is not for exact quantitative accuracy, as this would be a considerable challenge given the current state of theory. Instead we are after using theory and simulation to semiquantitatively screen different surface alloys.

Results and Discussion

NO Decomposition and Oxidation on Pt(100). Results of DFT−KMC calculations for NO reduction and NO oxidation at steady-state have been reported by the authors elsewhere.[14,27] The calculated TOF for N_2 and NO_2 formation are plotted as a function of temperature in Figure 1 at partial pressures of NO and O_2 of 0.468 Torr and 60.8 Torr, respectively. The TOF for N_2 formation increases with temperature. The apparent activation barrier for N_2 formation is calculated from these simulation results to be 7.4 kcal/mol.

DFT−KMC Approach to Kinetic Simulation

J. Phys. Chem. B, Vol. 109, No. 6, 2005 **2239**

The reaction orders for NO and O_2 were determined by running simulations at different partial pressures of NO and O_2, respectively. The resulting TOFs were subsequently plotted as a function of the log P_{NO} and log P_{O2} to establish the simulated reaction orders for NO and O_2 respectively. The calculated reaction orders for NO and O_2 were found to be 0.9 and −0.4 at 723 K and 0.55 and −0.06 at 773 K, respectively. These results indicate that oxygen inhibition of NO adsorption and NO decomposition is reduced at somewhat higher temperatures. There are two factors that can lead to this decrease in the NO reaction order as the temperature is increased from 723 to 773 K. The first is due to the self-inhibition by NO at moderate temperature, such as 773 K, where oxygen is no longer the dominant inhibitor. This is indicated by the increase in its oxygen reaction order from −0.4 to nearly 0. The decreased oxygen coverage leads to an increase in the relative NO coverage (the ratio of θ_{NO}/θ_O). NO can therefore begin to inhibit the rate thus leading to NO reaction orders that are less than one. These results are consistent with experimental results from Mummey and Schmidt[20] who studied NO decomposition in a high-pressure cell inside an ultrahigh vacuum chamber. They found that at low conversion (low P_{O2}) in an O_2 free-feed, the reaction of NO $\rightarrow$ N_2 is zero order in NO. At higher conversions, O_2 forms in the chamber and inhibits the rate. The rate then becomes first order in NO.

A second possible reason for the decrease in the NO reaction order over this temperature range is that the rate for NO_2 formation increases faster than the rate of N_2 formation up to 773 K. This decreases the selectivity to N_2 over this temperature range, which lowers the NO reaction order. As the temperature is increased beyond 773 K, the rate of NO_2 formation drops dramatically as the reaction becomes strongly equilibrium-limited, as was seen in Figure 1. The selectivity to N_2 then significantly increases and hence the reaction orders in NO increase.

The maximum found in NO_2 production is the result of the requirement that the reaction needs both adsorbed NO and O. At lower temperatures, the surface is predominantly covered by atomic oxygen. Little NO is able to adsorb on the surface. This subsequently limits the NO_2 formation rate. Increasing the temperature leads to a desorption of oxygen and thus allows NO to adsorb and react to form NO_2. At temperatures greater than 715 K, the surface coverages for both NO and O drop more rapidly, thus decreasing the amount of NO_2 that is formed. In addition, higher temperatures and an increased number of vacant sites significantly drive the reverse reaction where adsorbed NO_2 species are converted back into adsorbed NO and atomic oxygen. This is consistent with experimental results which indicate that NO_2 formation becomes thermodynamically limited at higher temperatures on Pt foils as well as on Pt particles supported on alumina catalysts.[20]

The calculated TOF values for N_2 formation found herein are higher than the experimental values measured under similar conditions. This may be expected for several reasons: (1) the simulation is for Pt(100), not polycrystalline Pt, both ultrahigh vacuum experiments as well as theory show that the NO dissociation is structure sensitive and that the (100) facets remove metal sharing in the transition state which significantly lowers the activation barrier;[27] (2) the proposed mechanism may still be incomplete; (3) the parameters used are not quite accurate enough; (4) the simulations do not account for support effects, defect sites, or other extrinsic features; (5) the Pt surface undergoes some oxidation when exposed to O_2 at high temperatures, which would decrease its intrinsic activity.[19] Despite the
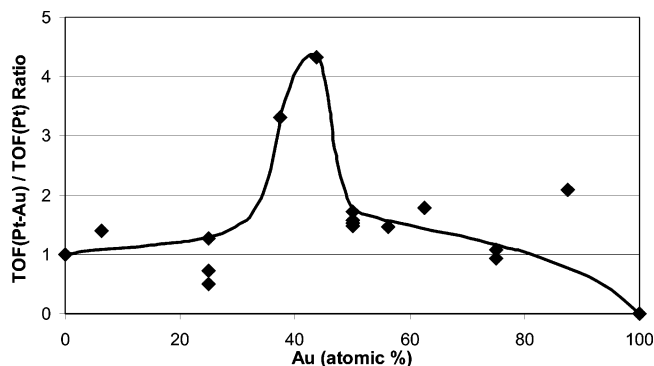
Figure 2. Ratio of TOF(Pt^{-1}s^{-1}) for Au−Pt(100) to TOF(Pt^{-1}s^{-1}) for Pt(100) as a function of Au content for the formation of N_2 at 713 K, [NO] = 0.456 Torr and [O_2] = 60.8 Torr. The turnover frequencies reported are on a per Pt atom basis since this is the active metal.

quantitative differences, the simulation results are still very valuable since they can establish relative trends when comparing different surfaces and reaction conditions as they provide insight into the effects of these parameters on the overall activity.

NO Decomposition and Oxidation on Pt−Au(100). The turnover frequency for N_2 formation (in units Pt^{-1} s^{-1}) was calculated on various Pt−Au(100) surfaces of increasing Au content at 713 K. The partial pressures of NO and O_2 were set equal to 0.456 and 60.8 Torr, respectively, to simulate lean conditions. The results, normalized to the TOF for Pt(100), are presented in Figure 2. In all of the simulations reported herein, we have assumed that the surface structure as well as the alloy composition and atomic arrangement remains stable throughout. Surface reconstruction and surface segregation are not explicitly modeled. It is likely that strongly bound surface species such as NO and oxygen will selectively pull Pt (to which it binds more strongly) to the surface, thus leading to an enrichment of Pt at the surface especially at higher temperatures. Chemisorbate-induced enrichment has been seen in a number of bimetallic systems at higher temperatures.[50−52] Under more extreme conditions Pt and Au may phase segregate. Our goal was not to model the phase changes that might occur but instead identify alloy phases that would be active if we could stabilize the specific atomic assemblies identified.

It is clear that the TOF for Pt−Au(100) increases with increasing Au content in the alloy and peaks at about 44% Au with a TOF value that is 4.3 times greater than the TOF on pure Pt(100). Since the calculated TOF on Au(100) is zero, Au is effectively acting here as an inert diluent of the active Pt metal. At 25 % Au, the two points in Figure 2 with TOF values that are much lower than that of the third point correspond to surfaces with different spatial arrangement of Pt and Au atoms. Images of the Pt−Au alloy surfaces that correspond to the peak in TOF in Figure 2 are shown in Figure 3. The behavior of the TOF for NO oxidation to NO_2 appears to be similar to that of N_2 formation. The TOF for NO oxidation shows a similar increase with increasing Au concentration.

The drop in the TOF for N_2 formation as the Au content increases from 43.8% to 50% coincides with the disappearance of Pt−Pt bridge sites (see Figure 3) which, based on the DFT results shown in Table 2, are the energetically favored sites for both NO and oxygen adsorption on the Pt(100) surface. In addition, it is important to note that the most active Pt−Au surface exhibits an arrangement of Pt atoms that does not include any 4-fold hollow Pt sites, which are the sites preferred for O_2 dissociative adsorption. This limits the amount of oxygen on the surface. These findings are similar to the experimental results by Panja and Koel[25] on a similar system Sn/Pt(100) alloy surface
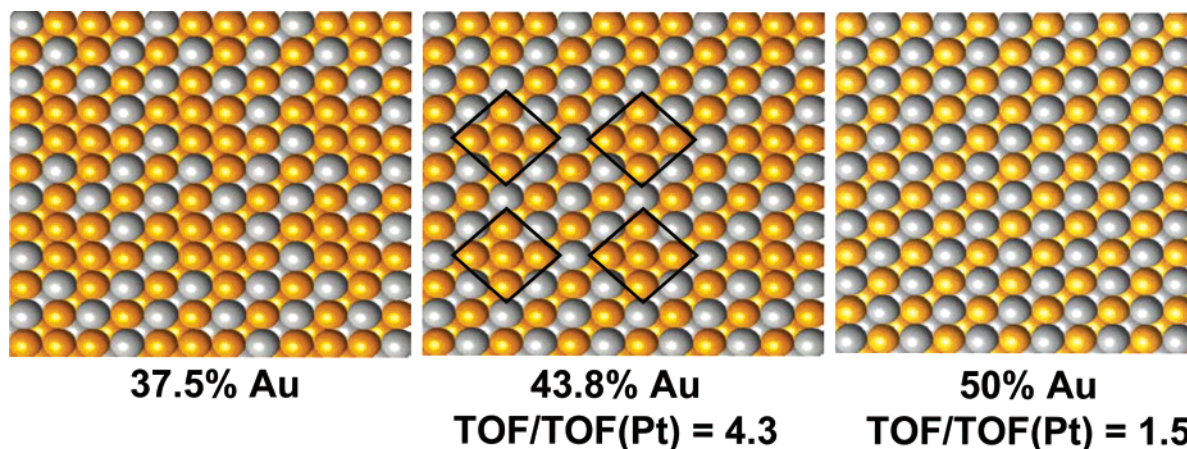
Figure 3. Representations of Pt–Au(100) alloy surfaces at different Au content and corresponding TOF of N_2 formation value normalized to TOF for Pt(100); the black square indicates the "+-site" Pt ensemble. (Au atoms are colored gray.)

where Sn forms c(2 × 2) and $(3\sqrt{2}x\sqrt{2})R45°$ surface structures. They indicate that Sn removes both the Pt-bridge and the 4-fold Pt sites. This significantly weakens the adsorption of NO which shuts down NO decomposition. The weaker NO adsorption on these surfaces, however, enhances the NO coupling reaction to form N_2O. Dinitrosyl surface complexes were identified from the high-resolution electron energy loss spectra on surfaces with high coverages of NO. In addition, they also agree with the results presented by Skelton et al.[24] for NO and O_2 adsorption and decomposition over Au deposited on Pt(335) substrates carried out at UHV conditions. The authors indicate that the addition of Au suppresses NO dissociation by poisoning step sites active for NO. Oxygen activation is also suppressed but to a much lower extent than NO.

The optimal site on the active $Pt_{56\%}Au_{44\%}$ surface involves a unique atomic arrangement of Pt atoms into a "+-site" ensemble where the Pt ensemble is surrounded by Au atoms, as shown by the black square in Figure 3. The site geometry maintains the Pt bridge sites necessary for NO adsorption but prevents the sites from being poisoned by oxygen. The central Pt atom contains only nearest-neighbor Pt atoms. We can therefore uniquely take advantage of the fact that the repulsive interactions between two adatoms are significantly higher than those between two NO molecules. This significantly limits the direct dissociation of O_2 and NO, thus avoiding oxygen inhibition and surface poisoning. In addition, it increases the likelihood of NO dimer formation and subsequent NO coupling to form N_2O. At higher temperatures N_2O reacts to form N_2 and a surface oxygen adatom.

The average binding energies (BE) of oxygen and NO were calculated for the same Pt–Au(100) surfaces under steady-state reaction conditions, and the values are plotted as a function of Au content in Figure 4. The average BE for atomic oxygen on Pt(100) is equal to 83.2 kcal/mol, which is much smaller than the intrinsic DFT value of 94.2 kcal/mol for the binding of oxygen on the favored Pt bridge site at zero coverage (Table 1). The BE for NO on Pt(100) under reaction conditions is equal to 35.5 kcal/mol, which is 15.7 kcal/mol less than the intrinsic value calculated from DFT (51.2 kcal/mol) for the bare Pt(100) surface. This indicates that lateral interactions between adsorbed species have a strong influence on binding energies.

The reported binding energies were averaged over all binding sites (Pt only, PtAu, and Au only) and over all time steps after the reaction reached steady state. It is important to note that these binding energy values take into account the effects of lateral interactions between adsorbed oxygen and surrounding
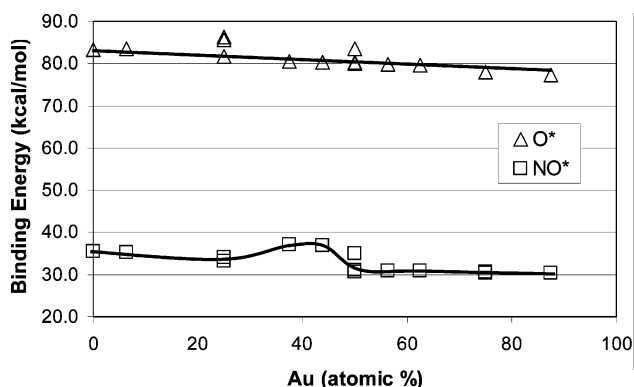
Figure 4. The average binding energies for NO* and O* on Pt–Au(100) surfaces as a function of Au atomic content under steady-steady NO reaction at 713 K, [NO] = 0.456 Torr and [O_2] = 60.8 Torr (solid lines are for visual aid only). The reported binding energies are averaged over the entire surface and therefore include contributions from species that sit at Pt-only, PtAu, and Au-only sites.

species at steady state as well as the nature of the adsorption site. Figure 4 shows that the addition of Au to Pt leads to a monotonic decrease in the average oxygen binding energy. The decrease in BE of oxygen results in an increase in TOF for surfaces with Au contents that are less than ∼44%. The two values of the BE of oxygen at 25% Au that are greater than the value for pure Pt correspond to the TOF values that are lower than those on pure Pt as is seen in Figure 2. This is consistent with the reported effect that an increase in the BE of oxygen leads to a decrease in the TOF. For surfaces with Au contents of 50% or greater, a further decrease in the BE of oxygen results in a decrease in the TOF of N_2 formation. The variations of the binding energy of NO as a function of Au content are different than those for atomic oxygen. The BE of adsorbed NO also decreases for surfaces with Au contents greater than 50%. Interestingly, there is an increase in the average NO binding energy over that on pure Pt when the composition of Au lies between 37.5% and 43.8%. This range corresponds to the region in Figure 2 where the TOF for N_2 formation goes through a maximum. This suggests that the increase in TOF of N_2 formation results from both a decrease in BE of oxygen as well as an increase in the BE of NO on the Pt–Au surfaces, which contain between 37.5 and 43.8% Au as compared to Pt. The stronger M–NO improves the likelihood of having higher concentrations of adsorbed NO that can react via NO coupling to form N_2O or N_2 and atomic O. The lower BE of oxygen results in a significant decrease in oxygen coverage as shown below.
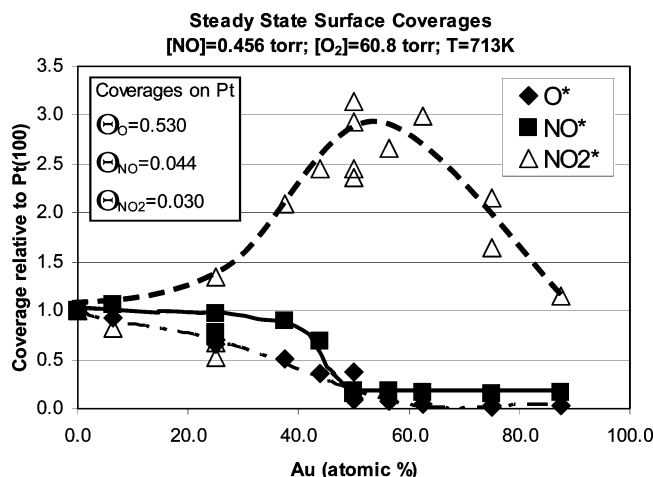
Figure 5. Effect of Au content on the calculated steady state coverage of NO*, O*, and NO₂* on Pt−Au(100) surfaces at 713 K, [NO] = 0.456 Torr, and [O₂] = 60.8 Torr (plotted lines are for visual aid only).

The steady-state surface coverages (in monolayers counting both Pt and Au atoms) of adsorbed NO (Θ_{NO}), adsorbed O (Θ_O), and adsorbed NO₂ (Θ_{NO2}) at 713 K and gas-phase partial pressures of NO and O₂ of 0.456 and 60.8 Torr, respectively, are plotted as a function of Au content in Figure 5. The plotted values are normalized to the simulated coverages found on the Pt(100) surface and as such are dimensionless values. The calculated coverages of N* and N₂O* are nearly zero. For comparison purposes, the calculated coverages of NO, O, NO₂ over pure Pt(100) are equal to 0.044, 0.530, and 0.030, respectively. Adsorbed oxygen is the most abundant surface species for surfaces where the Au content is below 50%. The coverage of atomic oxygen, Θ_O, decreases progressively with increasing Au content of the Pt−Au surface. The oxygen coverage is equal to 0.19 at 44% Au, where the TOF for N₂ formation peaks, and then drops sharply to 0.06 at 50% Au. The NO* surface coverage is significantly lower than the O* coverage. While Θ_{NO} also decreases with increasing Au content below 50%, the rate of its decrease is much less than that for Θ_O up until the Au content reaches 50% where, similar to Θ_O, it drops off considerably. The sharp decrease in Θ_{NO} and Θ_O at Au compositions of 50% can be correlated to the disappearance of Pt−Pt bridge sites on the alloy surface as shown in Figure 3. As Au increases, Θ_{NO2} increases. It peaks at about 50% Au where the surface coverage of NO₂ is approximately three times what it was on pure Pt(100). At Au contents above 50%, the absolute coverage of NO₂ is slightly greater than the coverage of atomic oxygen, whereas at Au contents below 50% the NO₂ surface coverages (Θ_{NO2}) are slightly lower than the coverages for NO (Θ_{NO}). The decrease in Θ_O is consistent with the decrease in BE of oxygen as Au content increases. The removal of surface oxygen (O*) by the associative desorption of O₂ and the oxidation of NO* to NO₂* frees up vacant sites for NO adsorption and reaction. The smaller decrease in Θ_{NO} and the corresponding more complex variations of BE of NO at Au contents below 50% suggest that lateral interactions between NO* and mainly O* have a significant effect on NO adsorption and reaction.

Snapshots of the surface adlayer for the most active Pt₅₆.₂%-Au₄₃.₈%(100) and the base Pt(100) surface at some instant in time after achieving steady state are compared in Figure 6. The surface oxygen concentration is significantly less on the alloy surface than on the Pt(100) surface. On the Pt₅₆.₂%Au₄₃.₈%(100) surface, oxygen predominantly adsorbs at the bridging Pt−Au sites. This particular alloy has no 4-fold hollow Pt sites, which
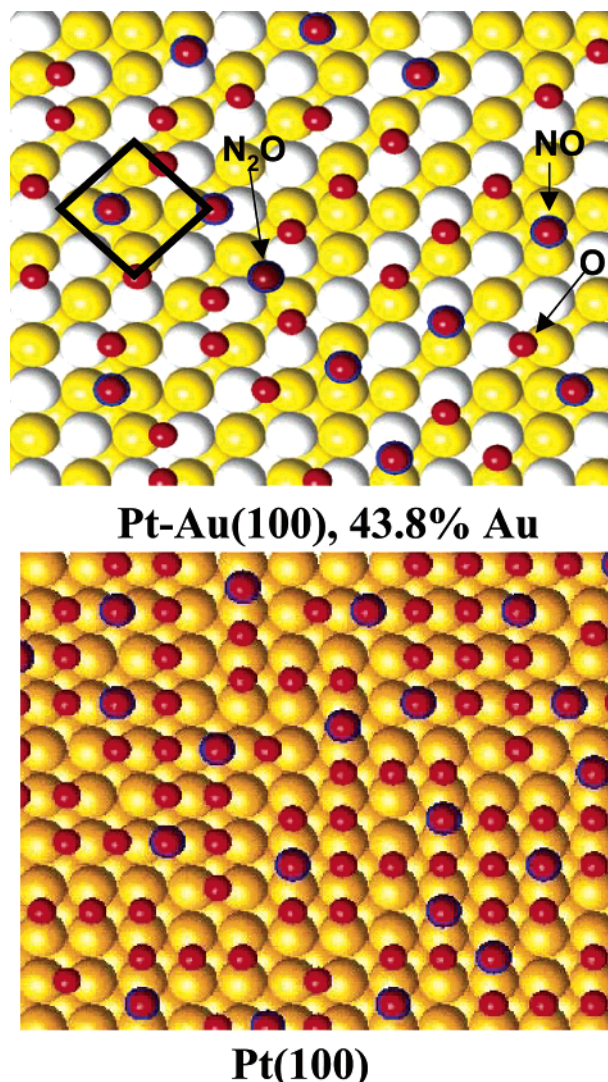
Figure 6. Representations of Pt(100) and Pt−Au(100) with 43.8% Au surfaces under reaction conditions at 713 K, [NO] = 0.456 Torr, and [O₂] = 60.8 Torr; the black square indicates a "+-site" Pt ensemble. (Au atoms are colored white).

are the sites that are thought to be responsible for O₂ and NO dissociation. The Pt "+"-sites are unique in that they predominantly allow for NO adsorption without necessarily having to share Pt atoms with coadsorbed oxygen. This is characteristically different than NO adsorption on the Pt(100) surface. The number and the strength of the lateral repulsive interactions that arise from metal atom sharing are much lower on the Pt₅₆.₂%Au₄₃.₈%-(100) alloy surface as compared to those on the Pt(100). This is the reason for the increased binding energy for NO on this alloy surface at steady state reaction conditions, as seen in Figure 4. DFT calculations showed that the binding energy of oxygen at the Pt bridge site drops by 7.4 kcal/mol when one of the Pt atoms in the bridge site is shared with a neighboring oxygen atom within the Pt "+"-site, which is highlighted with a black square in Figure 6. Similarly, the binding energy of NO is reduced by 8.6 kcal/mol when there is metal atom sharing with a neighboring oxygen atom within the "+" site. The addition of a second nearest neighbor oxygen atom to that same Pt ensemble results in a decrease in BE of oxygen by over 50 kcal/ mol. This is consistent with the fact that both NO* and O* do not like to share Pt atoms with other strongly bound ad-species. This will dramatically lower the surface coverage of oxygen, thus leading to a greater number of vacant sites around NO*

2242 *J. Phys. Chem. B, Vol. 109, No. 6, 2005*

Kieken et al.
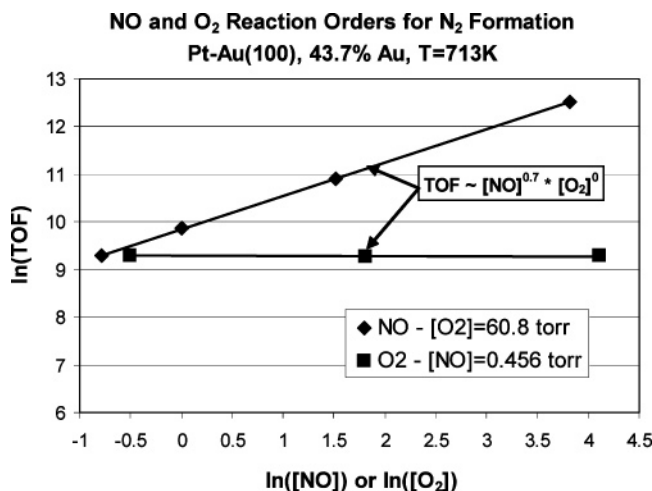
Figure 7. Simulated reaction orders of NO (◆) and O$_2$ (■) for the turnover frequency (Pt^{-1}s^{-1}) of N$_2$ formation on Pt−Au(100) containing 43.8% Au at 713 K, [NO] = 0.456 Torr (for O$_2$ reaction order), and [O$_2$] = 60.8 torr (for NO reaction order).

on the alloy surface as compared to Pt(100) which facilitates NO activation.

Reaction Kinetics. The reaction orders for NO and O$_2$ were calculated by changing the inlet partial pressures of [O$_2$] and [NO] and rerunning the simulations to determine their influence on the rate of N$_2$ formation at 713 K. We specifically examine the reaction order for the Pt$_{56.2\%}$Au$_{43.8\%}$(100) surface which exhibited the maximum TOF for N$_2$ formation, as was shown in Figure 2. The partial pressure of NO (O$_2$) was varied over a wide range of partial pressures at constant O$_2$ (NO) pressure of 60.8 (0.456) Torr to determine the NO (O$_2$) order. The results are shown in Figure 7. The reaction order for O$_2$ increases from −0.4 on Pt(100) to a value of zero on the Pt−Au(100) alloy. The rate on the Pt−Au(100) alloy does not appear to be inhibited by the presence of oxygen as it is on Pt(100) at 723 K.[14] The increase in the O$_2$ reaction order is consistent with the decrease in the coverage of adsorbed oxygen and the decrease in the BE of oxygen on the Pt−Au alloy surface as compared to Pt(100). The reaction order for NO decreases slightly from +0.9 on the Pt(100) at 723 K to +0.7 on the alloy surface at 713 K and identical O$_2$ concentrations. The subtle change in the simulated NO reaction order reflects the change in the steady-state concentrations of the different surface intermediates with increasing Au content as was described earlier.

A more detailed microkinetic analysis will be reported later in a separate publication to explain the change in the simulated reaction orders for the rate of N$_2$ formation on the alloy surface as compared to Pt. To better understand the kinetics over the alloy surface, we calculated the average forward, reverse, and net rates of reaction for all of the elementary steps monitored throughout the kinetic Monte Carlo simulations. The simulations were performed using a temperature 723 K and partial pressures of NO and O$_2$ of P$_{NO}$ = 0.468 Torr and P$_{O2}$ = 60.8 Torr over the Pt$_{56.2\%}$Au$_{43.8\%}$(100) surface. The results reported in Table 4 indicate that while oxygen removal via its reassociation or through NO oxidation appears to be more difficult, there is no one clear elementary step that limits the rate. On pure Pt(100), the net rate of NO coupling to form N$_2$O* was found to be between 5 and 10 times higher than the rate for direct NO dissociation into nitrogen and oxygen adatoms. Both coupling as well as direct NO dissociation, however, do appear to take place. A comparison of the rates for NO dissociation and NO

TABLE 4: Simulated forward, reverse, and net rates of reaction for individual elementary steps for the lean conversion of NO at T = 723 K and P_{NO} = 0.468 Torr and P_{O2} = 60.8 Torr

T = 723 K	net rate (s^{-1})	forward/reverse rates (s^{-1})
O$_2$(g) + 2* ⇌ O* + O*	7.23 × 10^4	1.36 × 10^5 (f) 6.33 × 10^4 (r)
N$_2$(g) + 2* ⇌ N* + N*	−	0.0 (f) 0.9 (r)
NO(g) + * ⇌ NO*	1.77 × 10^6	1.63 × 10^7 (f) 1.45 × 10^7 (r)
NO* + * ⇌ N* + O*	6.3 × 10^3	2.22 × 10^4 (f) 1.59 × 10^4 (r)
NO* + O* ⇌ NO$_2$* + *	5.59 × 10^5	6.50 × 10^5 (f) 9.12 × 10^4 (r)
NO* + N* ⇌ N$_2$O* + *	−	1.39 × 10^{-4} (f) 9.6 × 10^{-5}
NO* + NO* ⇌ N$_2$O* + O*	3.23 × 10^5	3.23 × 10^5 (f) 2.01 × 10^3 (r)
N$_2$O* ⇌ N$_2$(g) + O*	3.10 × 10^5	3.10 × 10^5 (f) 0.0 (r)
N$_2$O* ⇌ N$_2$O(g) + *	8.0 × 10^5	8.24 × 10^5 (f) 0.0 (r)
NO$_2$* ⇌ NO$_2$(g) + *	5.54 × 10^3	5.54 × 10^3 (f) 0.0 (r)

coupling over the Pt$_{56.2\%}$Au$_{43.8\%}$(100) surface, however, shows that the rate for NO coupling is now nearly 2 orders of magnitude greater on the Pt$_{56.2\%}$Au$_{43.8\%}$(100) alloy surface. The introduction of Au appears to shutdown the 4-fold Pt sites responsible for the direct dissociation of NO. NO coupling is therefore the dominant reaction path to N$_2$ formation on the alloy surface, which is consistent with the mechanism proposed by Amirnazmi et al.[18,19] In addition, the net rate of removal of O* from the surface by NO oxidation to NO$_2$ appears to be an order of magnitude greater than the rate of removal of O* by the associative desorption to O$_2$ on both Pt and Pt−Au surfaces. The oxidation of NO to NO$_2$ plays an important role in the removal of O*. The formation and decomposition of NO$_2$ has been reported to be a key step in the NO decomposition on Cu−ZSM-5 catalysts.[53,54] The rate of NO$_2$ formation however can be lowered significantly by operating at higher temperatures where the equilibrium takes over as was seen in the NO$_2$ TOF shown in Figure 1.

There are no experimental results that we are aware of for NO decomposition under lean conditions over Pt−Au surface alloys to which to compare our simulated kinetic results. The alloy surfaces constructed herein are likely difficult to synthesize since Pt and Au are not miscible in the bulk form at Au contents in the midrange.[55] Supported bimetallic Pt−Au clusters, however, can be prepared from bimetallic molecular clusters.[56] The preparation of Pt−Au bimetallic clusters that are stable under reaction conditions and that can mimic the Pt−Au surface shown in Figure 6 remains a significant challenge. There are, however, limited experimental results for the behavior of supported PtAu nanoparticles for the selective catalytic reduction of NO and the decomposition of NO over Au deposited over model Pt-(335) substrates under UHV conditions for NO$_x$ sensors. Amiridis et al. have studied the selective catalytic reduction of NO by propene on Pt−Au alloys.[23] They report that the addition of Au leads to a higher light-off temperature for NO decomposition. The increase in light-off temperature is likely the result of shutting down hydrocarbon activation sites. Direct NO decomposition sites are also likely to be shut down at higher Au concentrations. The work by Skelton et al.[24] indicates that the addition of Au onto a Pt(335) substrate blocks the active terrace sites, which dramatically decreases direct NO activation. Oxygen, however, can still dissociate over the open 111 terrace sites. Our simulation results are consistent with these findings in that Au shuts down the direct NO dissociation channels by removing the 4-fold Pt sites responsible for NO activation. Our results, however, are different in that we also see the suppression of O$_2$ adsorption as well as an increase in N$_2$ formation. These differences are most likely due to the differences in the alloy surface structure as well as differences in the actual reaction system. We have fabricated herein well-dispersed alloy surfaces where Au specifically breaks up Pt surface ensembles, thus

shutting down the 4-fold sites that are also necessary for activating O_2. In the experiments performed at low loadings of Au, Au is likely concentrated at the step edges where it shuts down sites for NO activation. O_2, however, can still be activated on the terrace sites which are comprised of Pt. At higher Au loadings, Pt is still likely enriched at the surface due to oxygen (or NO) induced reconstruction. The second difference between the experimental and simulation systems is the amount of N_2 that is formed. There is little to no N_2 that is formed experimentally when the Au composition is increased to greater than 50%. The simulations, however, show a reasonable steady-state N_2 production over the well-dispersed Pt−Au alloys. These differences are likely due to differences in the reaction conditions. The NO_x sensor experiments are carried out under ultrahigh vacuum conditions where NO coupling is not very likely. The simulations, however, are performed with a constant background partial pressure of NO and at a constant temperature, which is high enough to promote NO coupling. N_2O and N_2 formation is therefore much more likely.

Conclusions

Simulations of the steady-state decomposition of NO in excess molecular oxygen on Pt−Au(100) alloy surfaces show that increasing Au from 0 to about 44 atomic percent leads to an increase in the turnover frequency for N_2 formation. Dioxygen no longer inhibits the rate of N_2 formation on the most active alloy surface. This is due to a decrease in the oxygen binding energy and thus a decrease in oxygen coverage under reaction conditions. This results in an increase in the number of vacant sites available for NO adsorption. The maximum in turnover frequency occurs at 44% Au for the specific atomic assembly of Pt and Au into a special Pt "+-site". This specific arrangement of atoms removes the 4-fold hollow Pt sites that are preferred for both the dissociative adsorption of NO and O_2, but maintains neighboring Pt bridge sites for NO adsorption and NO coupling. The central Pt atom in the "+" ensemble contains only nearest-neighbor Pt atoms and can thus uniquely take advantage of the fact that the repulsive interactions between two oxygen atoms are significantly higher than those between two NO molecules, thus allowing for the formation of NO dimers while blocking oxygen poisoning. At Au contents equal to or greater than 50%, the turnover frequency of N_2 formation drops due to decreases in the NO binding energy and NO surface coverage. This also coincides with the disappearance of Pt bridge sites that are energetically preferred sites for NO as well as atomic oxygen.

The application of kinetic Monte Carlo simulation, in tandem with first-principle DFT calculations to generate the input kinetic data, provides a unique tool to screen *in silico* catalytic surfaces and relate systematic changes in the surface structure, composition, and atomic assemblies to changes in the catalytic activity, via changes in the rates of the underlying reaction elementary steps. This methodology may be quite useful in combinatorial or high-throughput efforts to guide catalyst development. For example in addition to Pt−Au, we have also screened various Pt−Cu and Pt−Ag alloy surfaces for NO decomposition and oxidation using this same kinetic Monte Carlo algorithm. The increase in the simulated turnover frequency of N_2 formation was lower for Pt−Ag, and even lower for Pt−Cu, than for Pt−Au. This is consistent with the decreasing affinity for oxygen of Cu, Ag, and Au, in that order.

References and Notes

(1) Caruthers, J. M.; Lauterbach, L. A.; Thomson, K. T.; Venkatasubramanian, V.; Snively, C. M.; Bhan, A.; Katare, S.; Oskarsdottir, G. *J. Catal.* **2003**, *216*, 98.
(2) Wolf, D.; Buyevskaya, O. V.; Baerns, M. *Appl. Catal. A Gen.* **2000**, *200*, 63.
(3) Buyevskaya, O. V.; Bruckner, A.; Kondratenko, E. V.; Wolf, D.; Baerns, M. *Catal. Today* **2001**, *67*, 369.
(4) Serra, J. M.; Corma, A.; Argente, E.; Valero, S.; Botti, V. *Appl. Catal. A* **2003**, *254*, 133.
(5) Cortright, R. D.; Dumesic, J. A. *Adv. Catal.* **2001**, *46*, 161.
(6) Boudart, M. *How To Speed Up The Development of Optimized Catalysts*, lecture given at the International Symposium on Frontiers in Catalysis in the 21st Century in Dehra Dun, India, 1999; and essay with same title, *Petroleum Asia*, 2000.
(7) Mei, D.; Hansen, E. W.; Neurock, M. *J. Phys. Chem. B* **2003**, *107*, 798.
(8) Hansen, E. W.; Neurock, M. *J. Phys. Chem. B* **2001**, *105*, 9218.
(9) Hansen, E. W.; Neurock, M. *J. Catal.* **2000**, *196*, 241.
(10) Hansen, E. W.; Neurock, M. *Chem. Eng. Sci.* **1999**, *54*, 3411.
(11) Hansen, E. W.; Neurock, M. *Surf. Sci.* **1999**, *441*, 410.
(12) Hansen, E. W.; Neurock, M. *Surf. Sci.* **2000**, *464*, 91.
(13) Neurock, M.; Mei, D. H. *Top. Catal.* **2002**, *20*, 5.
(14) Mei, D.; Ge, Q.; Kieken, L.; Lerou, J.; Neurock, M. *Molecular Phys.* **2004**, *102*, 4, 361.
(15) Li, Y.; Hall, W. K. *J. Catal.* **1991**, *129*, 202.
(16) Armor, J. N. *Catal. Today* **1995**, *26*, 99.
(17) Iwamoto, M.; Hamada, H. *Catal. Today* **1991**, *10*, 57.
(18) Amirnazmi, A.; Boudart, M. *J. Catal.* **1975**, *39*, 383.
(19) Amirnazmi, A.; Benson; J. E.; Boudart, M. *J. Catal.* **1973**, *30*, 55.
(20) Mummey, M. J.; Schmidt, L. D. *Surf. Sci.* **1981**, *109*, 29.
(21) Lam, Y. L.; Criado, J.; Boudart, M. *Nouv. J. Chim.* **1977**, *1*, 461.
(22) Wu, R. J.; Chou, T. Y.; Yeh, C. T. *Appl. Catal. B* **1995**, *6*, 105.
(23) Mihut, C.; Descorme, C.; Duprez, D.; Amiridis, M. D. *J. Catal.* **2002**, *212*, 125.
(24) Skelton, D. C.; Tobin, R. G.; Lambert, D. K.; DiMaggio, C. L.; Fisher, G. B. *Sens. Actuators B* **2003**, *96*, 46.
(25) Panja, C.; Koel, B. E. *J. Phys. Chem. A* **2000**, *104*, 2486.
(26) Masel, R. I. *Principles of Adsorption and Reaction on Solid Surfaces*, J. Wiley, Inc.: New York, 1996.
(27) Ge, Q.; Neurock, M. *J. Am. Chem. Soc.* **2004**, *126*, 1551.
(28) Hammer, B.; Norskov, J. K. *Adv. Catal.* **2000**, *45*, 71−129.
(29) Pirug, G.; Bonzel, H. P.; Hopster, H.; Ibach, J. *J. Chemi. Phys.* **1979**, *71*, 593.
(30) Gorte, R. J.; Schmidt, L. D.; Gland, J. L. *Surf. Sci.* **1981**, *109*, 367.
(31) Schwartz, S. B.; Fisher, G. B.; Schmidt, L. D. *J. Phys. Chem.* **1988**, *92*, 389.
(32) Olsson, L.; Persson, H.; Fridell, E.; Skoglundh, M.; Andersson, B. *J. Phys. Chem. B* **2001**, *105*, 6895.
(33) Eichler, A.; Hafner, J. *J. Catal.* **2001**, *204*, 118.
(34) Eichler, A.; Hafner, J. *J. Chem. Phys. Lett.* **2001**, *343*, 383.
(35) Brown, W. A.; King, D. A. *J. Phys. Chem. B* **2000**, *104*, 2578.
(36) Yeo, Y. Y.; Vattuone, L.; King, D. A. *J. Chem. Phys.* **1996**, *104*, 3810.
(37) Gland, J. L.; Sexton, B. A.; Fisher, G. B. *Surf. Sci.* **1980**, *95*, 587.
(38) Kresse, G.; Furthmuller, J. *Phys. Rev. B* **1996**, *54*, 11169.
(39) Kresse, G.; Hafner, J. *J. Phys.: Condens. Matter* **1994**, *6*, 8245.
(40) Perdew, J. P.; Chevary, J. A.; Vosko, S. H.; Jackson, K. A.; Pederson, M. R.; Singh, D. J.; Fiolhais, C. *Phys. Rev. B* **1992**, *46*, 6671.
(41) Mills, G.; Jonsson, H.; Schenter, G. K. *Surf. Sci.* **1995**, *324*, 305.
(42) Hopstaken, M. J. P.; Niemantsverdriet, J. W. *J. Phys. Chem. B* **2000**, *104*, 3058.
(43) Halgren, T. A. *J. Comput. Chem.* **1996**, *17*, 520.
(44) Shustorovich, E.; Sellers, H. *Surf. Sci. Rep.* **1998**, *31*, 1.
(45) Hansen, E. W. *Methodology for Stochastic Simulation of Surface Kinetics from First-Principles*, Ph.D. Thesis, Department of Chemical Engineering, University of Virginia, 2001.
(46) Dumesic, J. A.; Rudd, D. F.; Aparicio, L. M.; Reboske, J. E.; Trevino, A. A. *The Microkinetics of Heterogeneous Catalysis*; American Chemical Society: Washington, 1993; pp 39−42.

(47) van Santen, R. A.; Niemantsverdriet, J. W. *Chemical Kinetics and Catalysis*; Plenum Press: New York, 1995.

(48) Mullins and Weinberg; *Handbook of Heterogeneous Catalysis*; Wiley-VCH: New York, 1997; pp 972−983.

(49) Campbell, C. T. *Surf. Sci.* **1985**, *157*, 43.

(50) Tsong, T. T.; Ng, Y. S.; McLane, S. B., Jr. *J. Chem. Phys.* **1980**, *73*, 1464.

(51) Schwarz, J. A.; Polizzoti, R. S.; Burton, J. J. *J. Vac. Sci. Technol.* **1977**, *14*, 457.

(52) Bouwman, R.; Sachtler, W. M. H. *J. Catal.* **1970**, *19*, 127.

(53) Moden, B.; Da Costa, P.; Fonfe, B.; Lee, D. K.; Iglesia, E. *J. Catal.* **2002**, *209*, 75.

(54) Moden, B.; Da Costa, P.; Lee, D. K.; Iglesia, E. *J. Phys. Chem. B* **2002**, *106* (37), 9633.

(55) Gates, B. C.; Katzer, J. R.; Schuit, G. C. A. *Chemistry of Catalytic Processes*, McGraw-Hill Book Company: New York, 1979; pp 225−226.

(56) Chandler, D. D.; Schabel, A. B.; Pignolet, L. H. *J. Catal.* **2000**, *193*, 186.